Optimised optical fibre poling configurations: A numerical study

Francesco De Lucia[(1)], Pier Sazio[(1)*]
[(1)]*Optoelectronics Research Centre, University of Southampton, SO17 1BJ, UK*
pjas@soton.ac.uk

Abstract: We compare several thermal poling configurations, demonstrating that a single-anode geometry offers high effective Chi(2) even in optical fibers with loose manufacturing tolerances. Our modelling also reveals that PC fibers display an unexpected "inhibited poling" mechanism.
OCIS codes: (060.4370) Nonlinear optics, fibers; (230.4320) Nonlinear optical devices; (230.1150) All-optical devices; (000.4430) Numerical approximation and analysis.

1. Introduction

Thermal poling, invented at the beginning of the 90's by Myers et al. [1], is a method for creating a second order nonlinear optical response in centrosymmetric materials. Initially adopted for bulk glasses, the technique was later transferred to optical fibers, provided they were equipped with electrodes embedded inside cladding channels located adjacent to the fiber core [2]. Since then many different electrodes configurations have been explored and the conventional anode-cathode one has been replaced by a double-anode one, introduced for the first time by Margulis *et al.* in 2009 [3]. In 2014 De Lucia and co-workers implemented a new configuration (defined "induction poling" [4]), which, together with the use of liquid electrodes [5], presents an important step towards the possibility of poling optical fibers of any geometry, complexity and length with the final aim of creating efficient all-fiber quadratic nonlinear photonic devices, such as electro-optic modulators/switches, frequency converters, or sources of polarization-entangled photon pairs.

In this work we compare four different electrode configurations for thermal poling, including two already used to date, such as anode-cathode (A-C) [1] and double-anode (D-A) [3], plus two configurations never used before, namely single-anode (S-A) and floating-anode (F-A) via 2D-numerical models implemented using COMSOL™ Multiphysics, with the aim of identifying which is the most advantageous in terms of ease of poling and absolute value of the $\chi^{(2)}$ created inside the core.

2. Numerical model

The numerical simulations are developed from the 2D-model originally implemented by Camara *et al.* in 2014 [6] and subsequently modified by De Lucia *et al.* in 2016 [7]. The fiber geometry adopted is the same previously used for poling experiments in [4] and modeling in [7]. Two different types of charges (Na^+ and H_3O^+ (characterized by a 10^3 times smaller mobility [6])) are assumed to migrate under the effect of an externally applied electric field while negatively charged, non-bridging oxygen sites left behind (uncompensated negative charges) can be considered motionless at 300°C, and it is this charge separation that gives rise to the recorded field. When both migration and diffusion are taken into account, the local equation of continuity and Poisson's equation lead to the partial differential equation reported in [7]. Within our model, the fiber is located on top of a borosilicate microscope slide and the whole system is immersed in air and in the middle of a virtual metallic box whose walls (10 cm side length) are always held at ground potential.

The four different configurations of the electrodes have been implemented by simply assuming that in A-C, one of the electrodes is connected to a potential of +4.3 kV while the other is held at ground; in D-A configuration both electrodes are connected to +4.3 kV while only the virtual box walls are connected to ground; in S-A one of the electrodes is connected to +4.3 kV while the other is absent (hole empty), and finally in F-A one of the electrodes is connected to the potential of +4.3 kV while the other is left floating (not connected physically to any potential) with only the virtual box walls connected to ground while the other parameters of the poling process are identical. Fig. 1 (a) shows the trend of the effective $\chi^{(2)}$ created in the four different electrodes configurations. The $\chi^{(2)}$ in the D-A configuration exhibits a strong dependence on the relative position with respect to the center of the fiber and the nearest electrode. This behavior arises from the mutually competitive evolution of space-charge formation due to the presence of two anodes. In contrast, the single-anode configuration does not suffer from this issue and thus shows hardly any variation in the final effective $\chi^{(2)}$ value. Finally the A-C method is the least suitable because the final value of $\chi^{(2)}$ drops at half of its maximum value after the voltage applied is switched off, confirming the result presented in [3].

The general concept of electrostatic induction in which an embedded electrode connected to a HV source with one or more nearby embedded floating electrodes that generate space-charge regions (and consequently, second order nonlinearity) can be extended to fibers with a high degree of structural or geometric complexity, such as for example, solid-core Photonics Crystal Fibers (PCFs). Fig. 1 (b) and (c) show 2D numerical simulations of a fiber of this type, which as well as the microstructure surrounding the core, also contains an electrode filling the entire large hole in the fiber cladding. The first simulation in Fig. 1(b) shows the concentration distribution of the fast charges (Na^+) after 1380 s when the microstructure only contains air. It is clear that the temporal evolution of these cations is strongly inhibited in this area as they cannot penetrate the microstructure and solid core region. Importantly, we note that by uncovering this "inhibited poling" mechanism through numerical simulations, it is striking that this revealed behavior is consistent with the fact that there exist very few reports in the literature of experimental demonstrations of thermal poling in microstructured optical fibers [8], despite potentially attainable orders of magnitude improvements in SHG efficiency relative to conventional step-index poled optical fibers [9]. Significantly, in the second simulation shown in Fig. 1(c), we find that the "inhibited poling" mechanism can be defeated by incorporating floating conductors within the microstructure core area. In this electrostatic induction poling regime, a well-developed space-charge region begins to evolve as the cations can now effectively penetrate the PCF solid core.

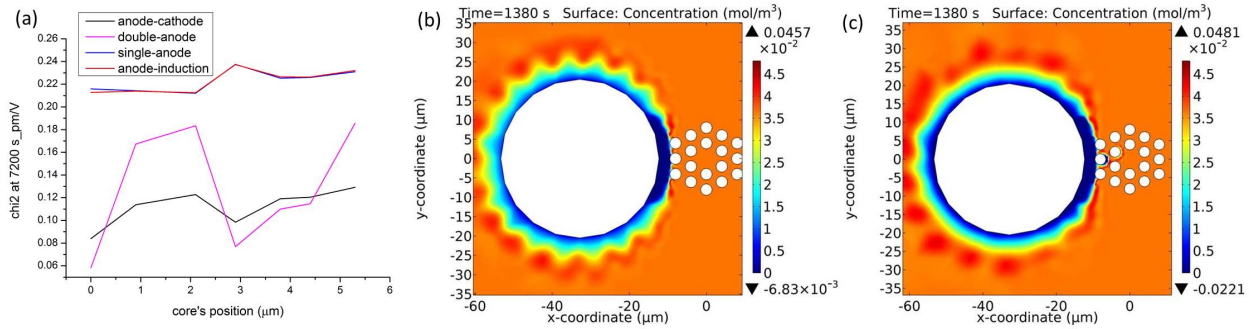

Fig. 1: (a) Trend of the value of $\chi^{(2)}$ calculated after 7200 s of poling for four different electrodes configurations, along the direction connecting the center of the fiber and one of the anodes. (b) Concentration of impurity charges (Na^+) after 1380 (S-A configuration, Vapp = + 2.5 kV, mobility and diffusion constant estimated for a temperature of 300 °C) for the thermal poling of a solid-core PCF. (b) Concentration of impurity charges (Na^+) calculated under the same conditions for thermal poling of a solid-core PCF except with two holes of the microstructure filled with a conductor and left floating during the poling process. The large cladding hole contains an electrode connected to the HV source.

3. Conclusion

In this work we present a numerical comparison between four different electrode configurations of optical fiber thermal poling and demonstrate that the single-anode configuration, which exhibits almost complete independence of the core-electrode relative position on the final effective $\chi^{(2)}$ value, is the optimal choice as it allows for relaxing manufacturing constraints during the drawing process of the fiber. The S-A configuration also shows the highest final value of $\chi^{(2)}$. We have also analyzed the temporal evolution of space-charge region formation in a solid core PCF and demonstrate that poling of the waveguide core is strongly inhibited when the PCF contains only air, but this limitation can be circumvented by the addition of embedded floating electrodes within the microstructured region as this enables localized electrostatic induction poling.

4. References

[1] R. A. Myers, N. Mukherjee, and S. R. J. Brueck, "Large second-order nonlinearity in poled fused silica," Opt. Lett. **16**, 1732-1734 (1991).
[2] 3. D. Wong, W. Xu, S. Fleming, M. Janos, and K-M Lo, "Frozen-in electrical field in thermally poled fibers," Opt. Fib. Tech. **5**, 235-241 (1999).
[3] W. Margulis, O. Tarasenko, and N. Myrén, "Who needs a cathode? Creating a second-order nonlinearity by charging glass fiber with two anodes," Opt. Express **17**, 15534-15540 (2009).
[4] F. De Lucia, D. Huang, C. Corbari, N. Healy and P. Sazio, "Optical fiber poling by induction," Opt. Lett. **39**, 6513-6516 (2014).
[5] F. De Lucia, D. W. Keefer, C. Corbari, and P. J. A. Sazio, "Thermal poling of silica optical fibers using liquid electrodes, " Opt. Lett. **42**,): 69-72 (2017).
[6] A. Camara, O. Tarasenko, and W. Margulis, "Study of thermally poled fibers with a two-dimensional model, " Opt. Express 22, 17700-17715 (2014).
[7] F. De Lucia, D. Huang, C. Corbari, N. Healy and P. Sazio, "Optical fiber poling by induction: analysis by 2D numerical modeling, " Opt. Lett. 41, 1700-1703 (2016).
[8] D. Faccio, A. Busacca, W. Belardi, V. Pruneri, P.G. Kazansky, T.M. Monro, D.J. Richardson, B. Grappe, M. Cooper and C.N. Pannell, "Demonstration of thermal poling in holey fibres", Electronics Lett. **37**, 107-108 (2001).
[9] T. M. Monro, V. Pruneri, N. G. R. Broderick, D. Faccio, P. G. Kazansky, and D. J. Richardson, "Broad-Band Second-Harmonic Generation in Holey Optical Fibers", IEEE Phot. Tech. Lett. **13**, 981-983 (2001).